Published in final edited form as:
Pain. 2008 August 15; 138(1): 47–60. doi:10.1016/j.pain.2007.11.004.

Effect of anti-NGF antibodies in a rat tibia fracture model of complex regional pain syndrome type I

Ilya Sabsovich[a,b], **Tzuping Wei**[a], **Tian-Zhi Guo**[a], **Rong Zhao**[a], **Xiaoyou Shi**[a], **Xiangqi Li**[b], **David C. Yeomans**[b], **Mikhail Klyukinov**[b], **Wade S. Kingery**[a,c], and **David J. Clark**[b,*]

a *Physical Medicine and Rehabilitation Service, Veterans Affairs Palo Alto Health Care System, Palo Alto, CA*

b *Anesthesiology Service, Veterans Affairs Palo Alto Health Care System Palo Alto, CA, and Department of Anesthesia, Stanford University School of Medicine, Stanford, CA*

c *Department of Orthopedic Surgery, Stanford University School of Medicine, Stanford, CA*

1. Introduction

Complex Regional Pain Syndrome (CRPS) has a low overall population prevalence (de Mos et al. 2007), but relatively high incidence after certain types of injuries. For example, distal tibial fractures are associated with a 31% incidence of CRPS type I (Sarangi et al. 1993). Many CRPS patients experience chronic pain and disability (Geertzen et al. 2006; Vaneker et al. 2006). Our group recently developed a model of CRPS (type I) based on distal tibial fracture and cast immobilization in rats (Guo et al. 2004). This model exhibits the classical signs of CRPS type I including allodynia, edema, warmth, and periarticular bone loss. There is also facilitated substance P (SP) signaling in the injured limb of this model (Guo et al. 2004; Guo et al. 2006) and in CRPS patients (Weber et al. 2001; Leis et al. 2003). Excessive SP signaling can directly induce keratinocyte nerve growth factor (NGF) expression and increase NGF levels in the skin of rodents (Amann et al. 2000; Burbach et al. 2001; Amann and Schuligoi 2004).

The roles for NGF and its tyrosine kinase A (TrkA) receptor in pain have been well characterized and recently reviewed (Pezet and McMahon 2006). Intraplantar (Amann et al. 1996a), intrathecal (Malcangio et al. 2000) and systemic administration of NGF (Bergmann et al. 1998) lead to nociceptive sensitization in rodents. Nerve growth factor supports nociception via several mechanisms including augmented primary afferent neurotransmitter production (Amann et al. 1996b), stimulation of sympathetic fiber ingrowth into the dorsal root ganglia (DRG's) (Ramer and Bisby 1999; Deng et al. 2000), and the activation of signaling systems like mitogen-activated protein kinase (MAPK) (Ji et al. 2002; Obata et al. 2004). Pain at the site of injection has been reported after administration of NGF to humans (McArthur et al. 2000; Svensson et al. 2003).

*Correspondence should be addressed to David J. Clark, M.D., PhD, Department of Anesthesiology (112A), Veterans Affairs Palo Alto Health Care System, 3801 Miranda Ave., Palo Alto, CA 94304, Tel: 650-493-5000 ext 67184, Fax: 650-852-3423, E-mail: djclark@stanford.edu.

Though some studies of NGF and TrkA in bone and bone-derived cells exist, little is understood about the significance of those effects with respect to the osteopenia seen in CRPS. One study by Asaumi et al. (Asaumi et al. 2000) demonstrated the expression of NGF and TrkA in several cell types surrounding healing fractures including osteoblasts and chondrocytes. The function of this bone-related NGF and TrkA expression remains uncertain as mice treated with a NGF sequestering antibody (anti-NGF) displayed less pain in a model of tumor-induced bone pain, yet the antibody did not influence tumor-induced bone remodeling, osteoblast proliferation or osteoclastogenesis (Halvorson et al. 2005).

The role of NGF with respect to edema in painful extremities is even less well understood. For example, early reports demonstrated that NGF could reverse edema caused by the injection of carrageenin, serotonin and dextran (Banks et al. 1984; Amico-Roxas et al. 1989). Later authors called into question this relationship in inflamed skin (Koltzenburg et al. 1999; Amann et al. 2002). Finally, the injection of NGF into unperturbed skin has been observed to cause rather than reduce edema (Schuligoi and Amann 1998). Thus the overall physiological circumstances may be important to the type of effect on edema NGF will display.

Using a newly developed anti-NGF antibody, we sought to determine how NGF functions in our CRPS model to alter some of the key features of this clinically important condition, namely nociceptive sensitization, bone loss, warmth and edema.

2. Materials and methods

These experiments were approved by our institute's Subcommittee on Animal Studies and followed the guidelines of the IASP (Zimmermann 1983). Adult (10-month-old) male Sprague Dawley rats (Harlan, Indianapolis, IN) were used in all experiments. The animals were housed individually in isolator cages with solid floors covered with 3 cm of soft bedding and were fed and watered ad libitum. During the experimental period the animals were fed Lab Diet 5012 (PMI Nutrition Institute, Richmond, IN), which contained 1.0% calcium, 0.5% phosphorus, and 3.3 IU/g of vitamin D3, and were kept under standard conditions with a 12-h light dark cycle.

2.1 Surgery

Tibia fracture was performed under isoflurane anesthesia as we have previously described (Guo et al. 2004). The right hindlimb was wrapped in stockinet (2.5 cm wide) and the distal tibia was fractured using pliers with an adjustable stop that had been modified with a 3-point jaw. The hindlimb wrapped in casting tape so the hip, knee and ankle were flexed. The cast extended from the metatarsals of the hindpaw up to a spica formed around the abdomen. To prevent the animals from chewing at their casts, the cast material was wrapped in galvanized wire mesh. The rats were given subcutaneous saline and buprenorphine immediately after procedure (0.03 mg/kg) and on the next day after fracture for postoperative hydration and analgesia. At 4 weeks the rats were anesthetized with isoflurane and the cast removed with a vibrating cast saw. All rats used in this study had union at the fracture site after 4 weeks of casting.

2.2 Drug

The anti-NGF antibody muMab 911 (Rinat Neuroscience, San Francisco, CA) is a TrkA-immunoglobulin G (TrkA-IGG) fusion molecule that binds to the NGF molecule, thus blocking the binding of NGF to the TrkA and p75 NGF receptors and inhibiting TrkA autophosphorylation (Hongo et al. 2000). Pharmacokinetic and behavioral experiments in rodents indicate that muMab 911 has a terminal half-life of 5–6 days in plasma and that a 10mg/kg dose administered every 5 or 6 days reduces nociceptive behavior in a variety of rodent

chronic pain models (Halvorson et al. 2005; Sevcik et al. 2005; Shelton et al. 2005; Jimenez-Andrade et al. 2007). Based on these data and discussions with lead scientists at Rinat Neuroscience it was decided to administer 10/mg/kg of muMab 911 via intraperitoneal injection on day 17 and day 24 after tibia fracture in rats. The drug was premixed at 4.1mg/ml.

2.3 RNA isolation and real-time PCR for NGF determination

The RNA was isolated from hindpaw skin and tibia bone using our previously described methods (Liang et al. 2003).. The purity and concentration of the purified RNA was determined spectrophotometrically. Complementary DNA (cDNA) was subsequently prepared using reverse transcriptase iScriptTM cDNA Synthesis Kit (Bio-Rad, Hercules, CA) according to the manufacturer's instruction. After incubation, the cDNA preparations were diluted 1:10 in DNase-free water prior to quantitative PCR (qPCR).

Real-time quantitative PCR (qPCR) was carried out using the SYBR® green reporter dye and protocol (Applied Biosystems; Foster City, CA). Briefly, 8 μl mineral oil was loaded at the bottom of each well to prevent loss of solution. 2.5 μl of 2× SYBR green and 0.5 μl of 10 μM NGF primers (forward primer: TGTGGACCCCAAACTGTTTAAGA; reverse primer: GTCTAAATCCAGAGTGTCCGAAGAG) were loaded with 2 μl diluted cDNA template in each well. Thermal cycling utilized an Applied Biosystems 7900HT system with a 5-min denaturation step at 95°C followed by 40 cycles of 95°C 30 sec/60°C 30 sec/72°C 60 sec). Melting curves were performed to document single product formation and agarose gel analysis was carried out to confirm the product size. The amplification of 18S RNA was used as an internal control. The 18S primers were purchased from Ambion (Austin, TX, USA). Amplification kinetics for the two amplification products was found to be similar. The data from real-time PCR experiments were analyzed by the comparative C_t method as described in the manual for the ABI Prism 7900 real-time system. Briefly, the parameter C_t was derived for each cDNA sample and primer pair; C_t is an expression of amplification kinetics referring to the cycle at which log-phase amplification reaches a pre-determined threshold. For a given sample, the C_t values for 18S RNA were subtracted from the C_t of NGF to arrive at a ΔC_t value. The mean ΔC_t from all control animal reactions was then subtracted from the mean ΔC_t for the treated samples to arrive at $\Delta\Delta C_t$. This parameter reflects the fold difference of over- or underexpression of NGF in fracture rat ipsilateral hindpaw skin or tibia bone tissue relative to control according to the expression $2^{-\Delta\Delta Ct}$. In each experiment samples were analyzed in triplicate or quadruplicate for the indicated numbers of rats.

2.4 Homogenization procedure and enzyme immunoassay for NGF, CGRP and SP

Rat hindpaw dorsal skin and proximal tibia were collected at 4 weeks after fracture and frozen immediately on dry ice. All tissues were cut into fine pieces in ice-cold phosphate buffered saline (PBS), pH 7.4, containing protease inhibitors (aprotinin (2 μg/ml), leupeptin (5 μg/ml), pepstatin (0.7 μg/ml), and PMSF (100 μg/ml); Sigma, St. Louis, MO, USA) followed by homogenization using a rotor/stator homogenizer. Homogenates were centrifuged for 5 min at 14 000 g, 4°C. Supernatants were transferred to fresh precooled Eppendorf tubes. Triton X-100 (Boehringer Mannheim, Germany) was added at a final concentration 0.01 %. The samples were centrifuged again for 5 min at 14 000g at 4°C. The supernatants were aliquoted and stored at −80°C. The NGF concentrations were determined by using the NGF Emax® ImmunoAssay System kit (Promega, Madison, WI) according to the manufacturer's instructions. The OD of the reaction product was read on a microplate reader at 450 nm, and values were normalized per gram of tissue assayed. The concentration of soluble NGF was calculated from the NGF standard curve. Positive and negative controls were included in each assay. NGF concentration was expressed as ng/mg protein.

NGF, CGRP and SP contents in the sciatic nerve were measured as we have previously described (Offley et al. 2005). Briefly, nerve samples were minced in 1 ml of 3:1 ethanol/0.7M HCl and homogenized for 20 s. The homogenates were shaken for 2 h at 4°C and centrifuged at 3000g for 20 min at 4°C. The supernatants were lyophilized and stored at −80°C. The lyophilized products were reconstituted with enzyme immunoassay (EIA) buffer before assay. After rehydration, the nerve extracts were assayed in duplicate using EIA kits (NGF Emax® ImmunoAssay System kit, Promega, Madison, WI; CGRP, 589001, Cayman Chemical, Ann Arbor, MI; and SP, 900018, Assay Designs, Ann Arbor, MI). Protein contents in all tissue extracts were measured by the Coomassie Blue Protein Assay Kit (Pierce, Rockford, IL).

2.5 Hindpaw nociception

To measure mechanical allodynia in the rats an up-down von Frey testing paradigm was used as we have previously described (Kingery et al. 2003; Guo et al. 2004; Guo et al. 2006). Rats were placed in a clear plastic cylinder (20 cm in diameter) with a wire mesh bottom and allowed to acclimate for 15 minutes. The paw was tested with 1 of a series of 8 von Frey hairs ranging in stiffness from 0.41 g to 15.14 g. The von Frey hair was applied against the hindpaw plantar skin at approximately midsole, taking care to avoid the tori pads. The fiber was pushed until it slightly bowed and then it was jiggled in that position for 6 seconds. Stimuli were presented at an interval of several seconds. Hindpaw withdrawal from the fiber was considered a positive response. The initial fiber presentation was 2.1 g and the fibers were presented according to the up-down method of Dixon to generate 6 responses in the immediate vicinity of the 50% threshold. Stimuli were presented at an interval of several seconds.

An incapacitance device (IITC Inc. Life Science. Woodland, CA) was used to measure hindpaw unweighting. The rats were manually held in a vertical position over the apparatus with the hindpaws resting on separate metal scale plates and the entire weight of the rat was supported on the hindpaws. The duration of each measurement was 6 seconds and 10 consecutive measurements were taken at 60-second intervals. Eight readings (excluding the highest and lowest ones) were averaged to calculate the bilateral hindpaw weight bearing values.

2.6 Hindpaw volume

A laser sensor technique was used to determine the dorsal-ventral thickness of the hindpaw, as we have previously described (Kingery et al. 2003; Guo et al. 2004; Guo et al. 2006). Before baseline testing the bilateral hindpaws were tattooed with a 2–3 mm spot on the dorsal skin over the midpoint of the third metatarsal. For laser measurements each rat was briefly anesthetized with isoflurane and then held vertically so the hindpaw rested on a table top below the laser. The paw was gently held flat on the table with a small metal rod applied to the top of the ankle joint. Using optical triangulation, a laser with a distance measuring sensor was used to determine the distance to the table top and to the top of the hindpaw at the tattoo site and the difference was used to calculate the dorsal-ventral paw thickness. The measurement sensor device used in these experiments (4381 Precicura, Limab, Goteborg, Sweden) has a measurement range of 200 mm with a 0.01 mm resolution.

2.7 Hindpaw temperature

The room temperature was maintained at 23°C and humidity ranged between 25–45%. The temperature of the hindpaw was measured using a fine wire thermocouple (Omega, Stanford, CT) applied to the paw skin, as previously described (Kingery et al. 2003; Guo et al. 2004; Guo et al. 2006). The investigator held the thermistor wire using an insulating Styrofoam block. Three sites were tested over the dorsum of the hindpaw; the space between the first and second metatarsals (medial), the second and third metatarsals (central), and the fourth and fifth metatarsals (lateral). After a site was tested in one hindpaw the same site was immediately tested in the contralateral hindpaw. The testing protocol was medial dorsum right then left,

central dorsum right then left, lateral dorsum right then left, medial dorsum left then right, central dorsum left then right, and lateral dorsum left then right. The six measurements for each hindpaw were averaged for the mean temperature.

2.8 Fos spinal cord immunohistochemistry

Rats were euthanized with CO2 and perfused intracardially with 200 ml 0.1 M PBS followed by 200 ml neutral 10% buffered formaldehyde. Spinal cord segments (L3–L5) were removed, post-fixed in the perfusion fixative overnight and cryoprotected in 30% sucrose at 4°C for 24 h. Serial frozen spinal cord sections, 40-μm-thick, were cut on a coronal plane by using a cryostat, collected in PBS, and processed as free floating sections. Fos immunostaining was performed as previously described (Sawamura et al. 2000; Kingery et al. 2001a). Because the sciatic nerve projects heavily to the L3-L5 segments of the spinal cord, we analyzed the numbers of Fos immunoreactive (Fos-IR) neurons at those levels.

To evaluate and compare the distribution of Fos positive neurons in the lumbar spinal cord, a Bioquant image analysis system (Bioquant, Nashville, TN) attached to a Nikon Eclipse 80i microscope was used. Digital images were captured using 10X magnification. The Fos-IR neurons were identified by dense black staining of the nucleus. The Fos-IR neurons were plotted and counted with Bioquant Automated Imaging module through four arbitrary defined regions of the spinal grey matter of the L3 - L5 segments, according to the cytoarchitectonic organization of the spinal cord (Rexed 1952; Molander et al. 1984); the superficial laminae (laminae I - II), the nucleus proprius (laminae III - IV), and the deep laminae (laminae V - VI; neck) of dorsal horn, and the ventral horn (laminae VII - X). For each section, the Fos-IR neurons were counted for each lamina, the counts were pooled, and the average number was calculated giving a count that was the mean of all stained neurons in those three sections per each cytoarchitectonic region. The investigator responsible for plotting and counting of the Fos-IR neurons wasblinded.

2.9 Microcomputed tomography (μCT)

Ex vivo scanning was performed for assessment of trabecular and cortical bone architecture using μCT (VivaCT 40, Scanco Medical AG, Basserdorf Switzerland). Specifically, trabecular bone architecture was evaluated at the distal femur and fourth lumbar vertebra and cortical bone morphology was evaluated at the femur midshaft. CT images were reconstructed in 1024 × 1024-pixel matrices for vertebral, distal femur, and midfemur samples and stored in 3-D arrays. The resulting grayscale images were segmented using a constrained Gaussian filter to remove noise, and a fixed threshold (25.5% of the maximal grayscale value for vertebrae and distal femur and 35% for midfemur cortical bone) was used to extract the structure of the mineralized tissue. The μCT parameters set at threshold = 255, $\sigma = 0.8$, support = 1 for vertebral samples, threshold = 255, $\sigma = 0.8$, support = 1 for distal femur, and threshold = 350, $\sigma = 1.2$, and support = 2 for midfemur evaluation analysis. A single operator outlined the trabecular bone region within distal femur and vertebral body, and cortical bone region in midfemur shaft.

Each L4 vertebral body was scanned using 223 transversely oriented 21μm thick slices (21-μm isotropic voxel size) encompassing a length of 4.68mm. The trabecular bone region was manually identified and all slices containing trabecular bone between the growth plates were included for analysis. In the distal femur 150 transverse slices of 21μm thickness (21-μm isotropic voxel size) encompassing a length of 3.15mm were acquired, but only 100 slices encompassing 2.1mm of the distal femur were evaluated, starting where the growth plate bridge across the middle of the metaphysis ends. The region of interest (ROI) was manually outlined on each CT slice, extending proximally from the growth plate. At the femur midshaft, 10 transverse CT slices were obtained, each 21 μm thick totaling 0.21 mm in length (21 μm

isotropic voxel size) and these were used to compute the cortical thickness (CTh, μm), bone perimeter (BPm, mm) bone marrow area (BMAr, mm2) and other cortical bone parameters.

2.10 Homogenization procedure and Bio-Plex Cytokine Analysis

The rat hindpaw dorsal skin collection and homogenization procedure was carried out as described in section 2.4. The supernatants were aliquoted, stored at −80 °C and assayed for TNFα, IL-1β, IL-6 and IL-10 cytokine levels using Bio-Rad Bio-Plex rat cytokine analysis kit in conjunction with the Bio-Plex system array reader according to the manufacturer's directions (Bio-Rad, Hercules, CA).

Briefly, samples and standards were added to the prewet beads that were dispensed into each well. After 30 min incubation and 3× washes, the beads were incubated with the detection antibodies for 30 min followed by 3× washes. Streptavidin-PE was then added to the beads prior to 3× washes and fluorescence reading. Each reaction in the kit was run in duplicate, with the experiment repeated three times. Standard curves for each of the analyzed substances were included in each run, and sample concentrations were automatically calculated. Cytokine concentration was expressed as pg/mg protein.

2.11 Study design

Baseline determinations were made of bilateral hindpaw temperature, thickness, mechanical nociceptive withdrawal thresholds, and weight bearing. After baseline tests the rats underwent a right distal tibia fracture with casting. The casts were removed after 28 days and repeat bilateral testing of hindpaw temperature, thickness, mechanical nociceptive withdrawal thresholds, and weighting bearing was performed. There were three treatment groups; control rats (no fracture), fracture rats that were injected with anti-NGF antibody, and fracture rats that were injected with vehicle on day 17 and day 24 after the fracture. Hindpaw temperature, thickness, and mechanical nociceptive thresholds data were analyzed as the difference between the treatment side and the contralateral untreated side. Right hindpaw weight bearing data were analyzed as a ratio between the right hindpaw weight and the sum of right and left hindpaws values ((2R/(R + L)) × 100%). Ex vivo μCT scanning was used to determine vertebral and femoral bone parameters for control rats (no fracture) and fracture rats that were injected with either the drug or vehicle. Spinal cord Fos protein expression was determined at 4 weeks after right tibia fracture.

The rats were tested on the 29th day after tibia fracture for behavioral, immunohistological, and biochemical outcomes; this was the day after cast removal and 5 days after the second dose of anti-NGF was given. This was in accordance with previous studies in rats with auto-immune arthritis where behavioral test was done 5 days after the last dose of anti-NGF was administered (Shelton et al. 2005). The rationale was to assess the beneficial drug effect when the maximal fracture induced behavioral changes were observed (Guo et al. 2004). We could reasonably expect that the anti-NGF would be active during the assessment period, but that the alterations characteristic of CRPS would have become manifest prior to the first dose of anti-NGF. Thus we did not seek to look at a preemptive effect but rather an effect of anti-NGF on established CRPS.

2.12 Statistical analysis

Statistical analysis was accomplished using a one-way analysis of variance (ANOVA) followed by *post hoc* Newman-Keuls multiple comparison testing to compare between control and fracture rats that were injected with either anti-NGF antibody or vehicle. All data are presented as the mean ± SE of the mean, and differences are considered significant at a p value less than 0.05 (Prism 4, GraphPad Software, San Diego, CA).

3. Results

3.1 Increased expression of NGF in hindpaw skin and tibia bone following distal tibia fracture and anti-NGF treatment

We used real-time PCR to detect changes in expression of NGF mRNA in hindpaw skin and tibia bone 4 weeks after fracture. Overall, we observed a significant increase in the mRNA levels in the ipsilateral hindpaw skin and tibia bone 28 days after fracture (Fig. 1A and 1B respectively). NGF mRNA levels were increased by 6-fold in the fracture group (n = 16) over control rats in hindpaw skin (n = 16; Fig. 1A) and by 3.6-fold in tibia bone (n = 8; Fig. 1B).

3.2 Anti-NGF effect on NGF production in hindpaw skin and tibia bone after distal tibia fracture

NGF protein levels were determined by EIA in hindpaw skin (Fig. 2A), proximal tibia (Fig. 2B) and sciatic nerve (data not shown) 4 weeks post-fracture. Baseline NGF levels were 5 fold higher in bone (46.01 ± 3.82 pg/mg protein) than in skin (9.28 ± 2.88 pg/mg protein). Rats were injected with either anti-NGF antibodies (n = 22) or vehicle (n = 18) at days 17 and 24 after the fracture. After fracture (n = 8) NGF protein levels increased 247.6% in the ipsilateral hindpaw skin and 177.6% in the ipsilateral tibia, relative to control rats (n = 8; Fig. 2A and 2B respectively). Nerve NGF levels did not significantly differ from control rats four weeks after fracture (data not shown) and basal levels were low (12.74 ± 2.46 pg/mg protein). Anti-NGF treatment reduced NGF protein levels in the hindpaw skin (n = 8, although it did not reach significance, Fig. 2A) and in tibia bone (n = 11; Fig. 2B) at 4 weeks after fracture. It is unclear if this was caused by reducing translation, increasing clearance of NGF, or binding and therefore making NGF immunological undetectable by EIA.

3.3 CGRP and SP expression in ipsilateral sciatic nerve after fracture and anti-NGF treatment

CGRP and SP protein levels were determined by EIA in sciatic nerve (Fig. 3) at 4 weeks post-fracture. Fracture increased both CGRP and SP levels (n = 9) in the ipsilateral sciatic nerve relative to control (n = 8). Anti-NGF treatment (n = 12) caused a significant decrease in CGRP and SP levels 4 weeks post-fracture (Fig. 3).

3.4 Anti-NGF effect on hindpaw vascular and nociceptive parameters after distal tibia fracture

The effects of anti-NGF treatment on fracture induced hindpaw warmth, edema, mechanical sensitivity and weight bearing were evaluated (Fig. 4). At 4 weeks post-fracture the right hindpaw edema (Fig. 4A) and temperature (Fig. 4B) were increased in the vehicle injected fracture rats compared to controls (n = 12). Anti-NGF increased hindpaw edema in the fracture limb, with no effect on warmth (Fig. 4A,B). Figure 4C illustrates that von Frey nociceptive thresholds in the right hindpaw were reduced after fracture, but anti-NGF treatment reversed development of this mechanical allodynia. Vehicle treated fracture rats unweighted the ipsilateral hindpaw by 62% at 4 weeks post-fracture and anti-NGF partially restored weight bearing in the fracture hindlimb (Fig. 4D).

Neither fracture nor anti-NGF treatment had any effect on nociceptive thresholds in the contralateral hindpaw *vs*. control rats (data not shown).

3.5 Anti-NGF effect on fracture induced Fos expression in lumbar spinal cord

Figure 5 depicts representative Fos immunostaining in the L3 – L5 dorsal horns in control rats (panels A and B, right and left sides respectively), vehicle treated fracture rats (C and D, ipsi- and contralateral sides respectively), and anti-NGF treated fracture rats (E anf F, ipsi- and contralateral sides respectively). Increased numbers of Fos positive neurons were observed in the ipsilateral and to a lesser extent the contralateral dorsal horn after fracture (5C, D) and this

was partially reversed by anti-NGF treatment (5E, F). Four weeks after the fracture Fos expression increased in the ipsilateral dorsal horn (Fig. 5C) in laminae I–II (475%), in laminae II–IV (277%), and in laminae V–VI (560%) (n = 6) compared to controls (Fig. 6A, B, C, respectively). Treatment with anti-NGF (n = 9) suppressed the increase in Fos-IR neurons in all ipsilateral dorsal horn laminae (Fig. 6A, B and C). In the contralateral dorsal horn of the fracture rats we observed a significant increase in Fos expression in all laminae (Fig. 6D, E and F), which was reduced in laminae I-II and V-VI by anti-NGF treatment (Fig. 6D and F).

3.6 Anti-NGF effect on trabecular and cortical bone loss after fracture

Figure 7 illustrates representative μCT scans demonstrating fracture induced trabecular bone loss in the distal femur and L_4 vertebrae which was partially reversed by anti-NGF treatment. Figure 8 shows quantitative data for the effects of fracture and anti-NGF treatment on trabecular bone. In the ipsilateral distal femur we observed a 66.6% loss of trabecular bone in the vehicle treated fracture group (n = 9) and a 52.9% reduction after anti-NGF treatment in fracture rats (n = 10) (Fig. 8A). In the contralateral distal femur (Fig. 8B) we found a 51.7% and 27.8% loss in the vehicle and drug treated fracture groups respectively. L_4 vertebral scan analysis shown a 38.4% loss in the vehicle treated and 37.2% in anti-NGF fracture rats (Fig. 8C).

Interestingly, we also observed changes in cortical bone parameters in this study (Fig. 9). Fracture decreased CTh both ipsi- (A) and contralaterally (D), whereas increased BPm ipsilaterally (B) and had a tendency to increase BPm contralaterally (E) and BMAr both ipsi- (C) and contralaterally (F). Anti-NGF blocked the effects of fracture on cortical bone ipsilaterally (panels A, B and C) and on BPm contralaterally (Fig. 9E). In addition, the drug had a tendency to oppose the fracture effect on CTh (D) and BMAr (F) contralaterally, which did not reach significance.

3.7 Increased expression of TNFα, IL-1β, IL-6 and IL-10 cytokines in hindpaw skin of fracture rats and anti-NGF effect on their levels

TNFα, IL-1β, IL-6 and IL-10 protein levels were determined by Bio-Plex in hindpaw skin (Fig. 10) at 4 weeks post-fracture. After fracture (n = 8) all four cytokines levels showed a trend to increase relative to controls (n = 8, Fig. 10), which was significant for IL-1β and IL-6 (Fig. 10B, C). Anti-NGF treated fracture rats demonstrated a significant elevation in these four cytokines (n = 8) relative to control and this cohort had elevated IL-1β and IL-10 levels compared to vehicle treated fracture rats (Fig. 10B and D).

3.8 Anti-NGF had no effect on body mass after fracture

We observed a body weight loss after 4 weeks in both fracture groups. At 4 weeks post-fracture the vehicle treated rats (n = 9) had lost 18% of their body mass, while the anti-NGF treated animals (n = 10) had lost 16% of their body weight. Unpaired t-test analysis showed a significant change for both of the fracture groups *vs.* control group (5% weight increase over 4 weeks, n = 8, data not shown), but there was no difference between vehicle and anti-NGF treated fracture groups.

4. Discussion

In these studies we attempted to define the role of NGF in the pathogenesis of various components of CRPS using a rat distal tibia fracture model. With respect to nociceptive sensitization we observed that anti-NGF antibodies could prevent mechanical nociceptive sensitization, increase weight bearing on the injured limb, reduce spinal cord dorsal horn Fos expression and reduce sciatic nerve neuropeptide content. It could be possible that anti-NGF is effective only in the presence of buprenorphine treatment since rats undergoing a fracture procedure were given buprenorphine for post-operative analgesia and anti-NGF antibodies for

chronic pain relief. However, buprenorphine pharmacokinetic studies in rats demonstrate that the drug is rapidly metabolized with a half-life of 7.73 ± 2.54 h (Megarbane et al. 2006). Buprenorphine elimination time makes it highly unlikely there could be any interaction of day 1 and day 2 buprenorphine injections with the anti-NGF antibodies which were administered on day 17 and 24 after fracture.

Positive effects were also observed in bone where anti-NGF treatment significantly inhibited distal femur bone loss after fracture. On the other hand, despite robust edema being measurable in this model we did not find evidence that anti-NGF antibody reduced the swelling or warmth found in hind paws ipsilateral to fracture. Likewise, while we predicted that anti-NGF treatment would be accompanied by reduced local cytokine levels, the skin levels of TNFα, IL-1β, IL-6 and the anti-inflammatory IL-10 were if anything enhanced after anti-NGF treatment. Thus the administration of anti-NGF after distal tibia fracture in rats reduces some but not all signs characteristic of CRPS.

While not necessarily focused on CRPS, many investigators have contributed to our understanding of how NGF supports nociceptive sensitization by focusing on primary afferent sensory nerve fiber function. For example, Malik-Hall et al. employing the technique of intradermal injection of NGF showed that the TrkA receptor on primary afferent neurons works through three major pathways to support hyperalgesia: extracellular signal-related kinase (ERK)/mitogen-activated protein kinase kinase (MEK), phosphatidylinositol 3-kinase (PI3K), and phospholipase Cγ (PLCγ) (Malik-Hall et al. 2005). Studies providing complementary results include those of Thompson who used an in vitro nerve-spinal cord preparation to observe an Aβ fiber wind-up in animals previously treated with NGF but not in controls (Thompson et al. 1995). Further evidence for the involvement of peripheral nerve fibers came from Kerr et al. who demonstrated the absence of NGF mediated hyperalgesia in mice lacking expression of Kv1.8 a sodium ion channel found on primary afferent neurons (Kerr et al. 2001). Finally, Herzberg et al. reported using the chronic constriction injury (CCI) model of neuropathic pain that the application of NGF antiserum at the site of the ligatures delayed the appearance of hyperalgesia (Herzberg et al. 1997).

Many groups have focused on the dorsal root ganglion (DRG) as a center for NGF-mediated effects on nociception. Cho et al. utilized the CFA model of chronic inflammation to demonstrate an increased expression of the P75 NGF receptor in DRG cells (Cho et al. 1996). Likewise, Obata et al. demonstrated an increase in DRG NGF content in the ventral rhizotomy nerve injury model, and in a model of lumbar disc herniation (Obata et al. 2002; Obata et al. 2004). While it is possible that this enhanced NGF signaling has direct effects on nociceptive processing, others have suggested that NGF's ability to enhance the expression of nociceptive neurotransmitters like CGRP or the expression of key nociceptive receptors like TRPV1 might play roles as well (Schuligoi and Amann 1998; Ji et al. 2002; Skoff et al. 2003; Skoff and Adler 2006). Our data fit well with these later observations. In the fracture model we observed a strong up-regulation of CGRP and SP in sciatic nerve ipsilateral to the injury. Anti-NGF antibody reduced both CGRP and SP in these nerves thus providing one possible mechanism whereby anti-NGF reduces nociceptive sensitization in this model.

We originally hypothesized that anti-NGF would reduce the elevated levels of cytokines in skin observed after tibia fracture. Elevations of several cytokines have been observed in patients suffering from CRPS (Groeneweg et al. 2006). Our data, however, demonstrated that anti-NGF actually increases the abundance of TNFα, IL-1β and the anti-inflammatory IL-10 while leaving the concentration of IL-6 unchanged in the hind paw skin of rats after fracture despite reductions in nociceptive sensitization. Similar results were provided by Shelton et al. who using CFA-induced model of arthritis observed that anti-NGF antibodies enhanced IL-1β accumulation in affected paws despite reducing nociceptive sensitization (Shelton et al.

2005). Our observations suggest that NGF contributes to nociceptive sensitization by mechanisms other than regulation of local cytokine production. This could be the case if, for example, NGF exerted most of its pro-nociceptive influence at the level of the DRG as discussed above. It is possible, of course that cytokines are involved in CRPS, but that the location of the relevant expression is not in skin but the CNS as has been suggested by others (Alexander et al. 2006).

Patchy osteopenia in the periarticular area along with bone edema is commonly observed in patients with CRPS (Genant et al. 1975; Sintzoff et al. 1997; Kim et al. 2003), though to a lesser degree and in a more delayed fashion in the contralateral limb (Kozin et al. 1976). One analysis suggested that CRPS affects the trabecular bone to a greater extent than cortical bone (Bickerstaff et al. 1993). The bone-related changes in our model of CRPS match these clinical observations well. For example, we observed a reduction in bone density largest on the ipsilateral fracture side, but measurable bilaterally. Furthermore, the changes we observed in trabecular bone were far greater than in cortical bone. As for the effects of anti-NGF, a small but significant effect of anti-NGF to reduce trabecular bone loss was observed in the distal femur, and essentially no anti-NGF effect was seen on vertebrae.

The mechanism for these changes is somewhat unclear. One explanation is that the rats when treated with anti-NGF placed greater weight on the fractured hind limb as is suggested by the hind paw weight bearing data. Indeed, disuse and immobilization are recognized causes of bone loss (del Puente et al. 1996). However, these changes were also observed contralaterally, which is inconsistent with this purely mechanical mechanism. There are other data suggesting that NGF might alter bone mineral density by acting on bone cells themselves. For example, after rib fracture, NGF and its cognate TrkA receptor were observed in most bone forming cells near the fracture callus (Asaumi et al. 2000). Unfortunately, the precise effects of NGF on bone formation are poorly understood at this point.

While we observed positive effects of anti-NGF on nociception and to a limited degree on bone loss, anti-NGF treatment failed to significantly reduce hind paw warmth and edema. There is clinical and preclinical evidence that edema characteristic of CRPS results from facilitated protein extravasation mediated by the release of SP from the terminals of C-fibers (Oyen et al. 1993; Kingery et al. 2001b; Weber et al. 2001; Guo et al. 2004). It might have been expected that the reduction in sciatic nerve neuropeptides by anti-NGF would reduce the edema in the fractured hind paw. We did not observe this. The facilitated effects of SP to promote extravasation in CRPS are likely due to post-junctional changes (Leis et al. 2003) such as enhanced signaling through the SP NK1 receptors, or possibly by reduced activity of the SP degrading enzyme neutral endopeptidase (NEP) (Kingery et al. 2001b; Leis et al. 2003; Guo et al. 2006). Thus the anti-NGF mediated reductions in fracture-enhanced SP levels may not be sufficient to reduce hind paw edema. Furthermore, cytokines such as IL-1β and IL-6 have been shown to contribute to edema when present in the skin (Nedrebo et al. 1999). In fact, anti-NGF treatment increased levels of skin cytokines, a possible mechanism for the enhanced edema caused by anti-NGF treatment in our experiments. Again, Shelton et al. observed enhanced edema in CFA-induced arthritis when animals were exposed to anti-NGF antibodies, consistent with our results (Shelton et al. 2005).

In summary, these studies show that anti-NGF administered after tibia fracture exerts a strong anti-nociceptive effect, a modest sparing effect on bone loss and no ability to reduce vascular abnormalities or cytokine production. The antinociceptive effects may relate to the ability of this antibody to reduce peripheral nerve SP and CGRP content or to a direct inhibitory effect on the elevated NGF levels observed after fracture. The differential effects of anti-NGF on different manifestations of CRPS strongly underscore the multiple mechanisms activated in this condition that correspond to the plethora of changes observed clinically and in our model.

As pain is the chief complaint associated with CRPS and the chief cause of disability, it would appear that anti-NGF may prove to be a valuable agent in the treatment of this syndrome and possibly other types of chronic inflammatory pain.

Acknowledgements

This study was supported by National Institutes of Health Grants GM65345 and DK67197. We would also like to thank Rinat Neuroscience for generously providing anti-NGF antibodies.

References

Alexander GM, Perreault MJ, Reichenberger ER, Schwartzman RJ. Changes in immune and glial markers in the CSF of patients with Complex Regional Pain Syndrome. Brain Behav Immun. 2006

Amann R, Egger T, Schuligoi R. The tachykinin NK(1) receptor antagonist SR140333 prevents the increase of nerve growth factor in rat paw skin induced by substance P or neurogenic inflammation. Neuroscience 2000;100(3):611–615. [PubMed: 11098124]

Amann R, Lanz I, Schuligoi R. Effects of morphine on oedema and tissue concentration of nerve growth factor in experimental inflammation of the rat paw. Pharmacology 2002;66(3):169–172. [PubMed: 12372907]

Amann R, Schuligoi R. Beta adrenergic inhibition of capsaicin-induced, NK1 receptor-mediated nerve growth factor biosynthesis in rat skin. Pain 2004;112(1–2):76–82. [PubMed: 15494187]

Amann R, Schuligoi R, Herzeg G, Donnerer J. Intraplantar injection of nerve growth factor into the rat hind paw: local edema and effects on thermal nociceptive threshold. Pain 1996a;64(2):323–329. [PubMed: 8740610]

Amann R, Sirinathsinghji DJ, Donnerer J, Liebmann I, Schuligoi R. Stimulation by nerve growth factor of neuropeptide synthesis in the adult rat in vivo: bilateral response to unilateral intraplantar injections. Neurosci Lett 1996b;203(3):171–174. [PubMed: 8742020]

Amico-Roxas M, Caruso A, Leone MG, Scifo R, Vanella A, Scapagnini U. Nerve growth factor inhibits some acute experimental inflammations. Arch Int Pharmacodyn Ther 1989;299:269–285. [PubMed: 2774768]

Asaumi K, Nakanishi T, Asahara H, Inoue H, Takigawa M. Expression of neurotrophins and their receptors (TRK) during fracture healing. Bone 2000;26(6):625–633. [PubMed: 10831935]

Banks BE, Vernon CA, Warner JA. Nerve growth factor has anti-inflammatory activity in the rat hindpaw oedema test. Neurosci Lett 1984;47(1):41–45. [PubMed: 6462528]

Bergmann I, Reiter R, Toyka KV, Koltzenburg M. Nerve growth factor evokes hyperalgesia in mice lacking the low-affinity neurotrophin receptor p75. Neurosci Lett 1998;255(2):87–90. [PubMed: 9835221]

Bickerstaff DR, Charlesworth D, Kanis JA. Changes in cortical and trabecular bone in algodystrophy. Br J Rheumatol 1993;32(1):46–51. [PubMed: 8422559]

Burbach GJ, Kim KH, Zivony AS, Kim A, Aranda J, Wright S, Naik SM, Caughman SW, Ansel JC, Armstrong CA. The neurosensory tachykinins substance P and neurokinin A directly induce keratinocyte nerve growth factor. J Invest Dermatol 2001;117(5):1075–1082. [PubMed: 11710915]

Cho HJ, Park EH, Bae MA, Kim JK. Expression of mRNAs for preprotachykinin and nerve growth factor receptors in the dorsal root-ganglion following peripheral inflammation. Brain Res 1996;716(1–2):197–201. [PubMed: 8738239]

de Mos M, de Bruijn AG, Huygen FJ, Dieleman JP, Stricker BH, Sturkenboom MC. The incidence of complex regional pain syndrome: a population-based study. Pain 2007;129(1–2):12–20. [PubMed: 17084977]

del Puente A, Pappone N, Mandes MG, Mantova D, Scarpa R, Oriente P. Determinants of bone mineral density in immobilization: a study on hemiplegic patients. Osteoporos Int 1996;6(1):50–54. [PubMed: 8845600]

Deng YS, Zhong JH, Zhou XF. Effects of endogenous neurotrophins on sympathetic sprouting in the dorsal root ganglia and allodynia following spinal nerve injury. Exp Neurol 2000;164(2):344–350. [PubMed: 10915573]

Geertzen JH, Van Wilgen CP, Schrier E, Dijkstra PU. Chronic pain in rehabilitation medicine. Disabil Rehabil 2006;28(6):363–367. [PubMed: 16492632]

Genant HK, Kozin F, Bekerman C, McCarty DJ, Sims J. The reflex sympathetic dystrophy syndrome. A comprehensive analysis using fine-detail radiography, photon absorptiometry, and bone and joint scintigraphy. Radiology 1975;117(1):21–32. [PubMed: 51504]

Groeneweg JG, Huygen FJ, Heijmans-Antonissen C, Niehof S, Zijlstra FJ. Increased endothelin-1 and diminished nitric oxide levels in blister fluids of patients with intermediate cold type complex regional pain syndrome type 1. BMC Musculoskelet Disord 2006;7:91. [PubMed: 17137491]

Guo TZ, Offley SC, Boyd EA, Jacobs CR, Kingery WS. Substance P signaling contributes to the vascular and nociceptive abnormalities observed in a tibial fracture rat model of complex regional pain syndrome type I. Pain 2004;108(1–2):95–107. [PubMed: 15109512]

Guo TZ, Wei T, Kingery WS. Glucocorticoid inhibition of vascular abnormalities in a tibia fracture rat model of complex regional pain syndrome type I. Pain 2006;121(1–2):158–167. [PubMed: 16472917]

Halvorson KG, Kubota K, Sevcik MA, Lindsay TH, Sotillo JE, Ghilardi JR, Rosol TJ, Boustany L, Shelton DL, Mantyh PW. A blocking antibody to nerve growth factor attenuates skeletal pain induced by prostate tumor cells growing in bone. Cancer Res 2005;65(20):9426–9435. [PubMed: 16230406]

Herzberg U, Eliav E, Dorsey JM, Gracely RH, Kopin IJ. NGF involvement in pain induced by chronic constriction injury of the rat sciatic nerve. Neuroreport 1997;8(7):1613–1618. [PubMed: 9189901]

Hongo JS, Laramee GR, Urfer R, Shelton DL, Restivo T, Sadick M, Galloway A, Chu H, Winslow JW. Antibody binding regions on human nerve growth factor identified by homolog- and alanine-scanning mutagenesis. Hybridoma 2000;19(3):215–227. [PubMed: 10952410]

Ji RR, Samad TA, Jin SX, Schmoll R, Woolf CJ. p38 MAPK activation by NGF in primary sensory neurons after inflammation increases TRPV1 levels and maintains heat hyperalgesia. Neuron 2002;36 (1):57–68. [PubMed: 12367506]

Jimenez-Andrade JM, Martin CD, Koewler NJ, Freeman KT, Sullivan LJ, Halvorson KG, Barthold CM, Peters CM, Buus RJ, Ghilardi JR, Lewis JL, Kuskowski MA, Mantyh PW. Nerve growth factor sequestering therapy attenuates non-malignant skeletal pain following fracture. Pain. 2007

Kerr BJ, Souslova V, McMahon SB, Wood JN. A role for the TTX-resistant sodium channel Nav 1.8 in NGF-induced hyperalgesia, but not neuropathic pain. Neuroreport 2001;12(14):3077–3080. [PubMed: 11568640]

Kim SH, Chung SK, Bahk YW, Chung YA, Song KS. 99mTc-HDP pinhole SPECT findings of foot reflex sympathetic dystrophy: radiographic and MRI correlation and a speculation about subperiosteal bone resorption. J Korean Med Sci 2003;18(5):707–714. [PubMed: 14555825]

Kingery WS, Agashe GS, Sawamura S, Davies MF, Clark JD, Maze M. Glucocorticoid inhibition of neuropathic hyperalgesia and spinal Fos expression. Anesth Analg 2001a;92(2):476–482. [PubMed: 11159254]

Kingery WS, Davies MF, Clark JD. A substance P receptor (NK1) antagonist can reverse vascular and nociceptive abnormalities in a rat model of complex regional pain syndrome type II. Pain 2003;104 (1–2):75–84. [PubMed: 12855316]

Kingery WS, Guo T, Agashe GS, Davies MF, Clark JD, Maze M. Glucocorticoid inhibition of neuropathic limb edema and cutaneous neurogenic extravasation. Brain Res 2001b;913(2):140–148. [PubMed: 11549377]

Koltzenburg M, Bennett DL, Shelton DL, McMahon SB. Neutralization of endogenous NGF prevents the sensitization of nociceptors supplying inflamed skin. Eur J Neurosci 1999;11(5):1698–1704. [PubMed: 10215923]

Kozin F, Genant HK, Bekerman C, McCarty DJ. The reflex sympathetic dystrophy syndrome. II. Roentgenographic and scintigraphic evidence of bilaterality and of periarticular accentuation. Am J Med 1976;60(3):332–338. [PubMed: 56892]

Leis S, Weber M, Isselmann A, Schmelz M, Birklein F. Substance-P-induced protein extravasation is bilaterally increased in complex regional pain syndrome. Exp Neurol 2003;183(1):197–204. [PubMed: 12957502]

Liang D, Li X, Lighthall G, Clark JD. Heme oxygenase type 2 modulates behavioral and molecular changes during chronic exposure to morphine. Neuroscience 2003;121(4):999–1005. [PubMed: 14580950]

Malcangio M, Ramer MS, Boucher TJ, McMahon SB. Intrathecally injected neurotrophins and the release of substance P from the rat isolated spinal cord. Eur J Neurosci 2000;12(1):139–144. [PubMed: 10651868]

Malik-Hall M, Dina OA, Levine JD. Primary afferent nociceptor mechanisms mediating NGF-induced mechanical hyperalgesia. Eur J Neurosci 2005;21(12):3387–3394. [PubMed: 16026476]

McArthur JC, Yiannoutsos C, Simpson DM, Adornato BT, Singer EJ, Hollander H, Marra C, Rubin M, Cohen BA, Tucker T, Navia BA, Schifitto G, Katzenstein D, Rask C, Zaborski L, Smith ME, Shriver S, Millar L, Clifford DB, Karalnik IJ. A phase II trial of nerve growth factor for sensory neuropathy associated with HIV infection. AIDS Clinical Trials Group Team 291. Neurology 2000;54(5):1080–1088. [PubMed: 10720278]

Megarbane B, Hreiche R, Pirnay S, Marie N, Baud FJ. Does high-dose buprenorphine cause respiratory depression?: possible mechanisms and therapeutic consequences . Toxicol Rev 2006;25(2):79–85. [PubMed: 16958555]

Molander C, Xu Q, Grant G. The cytoarchitectonic organization of the spinal cord in the rat. I. The lower thoracic and lumbosacral cord. J Comp Neurol 1984;230(1):133–141. [PubMed: 6512014]

Nedrebo T, Berg A, Reed RK. Effect of tumor necrosis factor-alpha, IL-1beta, and IL-6 on interstitial fluid pressure in rat skin. Am J Physiol 1999;277(5 Pt 2):H1857–1862. [PubMed: 10564140]

Obata K, Tsujino H, Yamanaka H, Yi D, Fukuoka T, Hashimoto N, Yonenobu K, Yoshikawa H, Noguchi K. Expression of neurotrophic factors in the dorsal root ganglion in a rat model of lumbar disc herniation. Pain 2002;99(1–2):121–132. [PubMed: 12237190]

Obata K, Yamanaka H, Dai Y, Mizushima T, Fukuoka T, Tokunaga A, Noguchi K. Activation of extracellular signal-regulated protein kinase in the dorsal root ganglion following inflammation near the nerve cell body. Neuroscience 2004;126(4):1011–1021. [PubMed: 15207334]

Offley SC, Guo TZ, Wei T, Clark JD, Vogel H, Lindsey DP, Jacobs CR, Yao W, Lane NE, Kingery WS. Capsaicin-sensitive sensory neurons contribute to the maintenance of trabecular bone integrity. J Bone Miner Res 2005;20(2):257–267. [PubMed: 15647820]

Oyen WJ, Arntz IE, Claessens RM, Van der Meer JW, Corstens FH, Goris RJ. Reflex sympathetic dystrophy of the hand: an excessive inflammatory response? Pain 1993;55(2):151–157. [PubMed: 8309706]

Pezet S, McMahon SB. Neurotrophins: mediators and modulators of pain. Annu Rev Neurosci 2006;29:507–538. [PubMed: 16776595]

Ramer MS, Bisby MA. Adrenergic innervation of rat sensory ganglia following proximal or distal painful sciatic neuropathy: distinct mechanisms revealed by anti-NGF treatment. Eur J Neurosci 1999;11(3):837–846. [PubMed: 10103077]

Rexed B. The cytoarchitectonic organization of the spinal cord in the cat. J Comp Neurol 1952;96(3):414–495. [PubMed: 14946260]

Sarangi PP, Ward AJ, Smith EJ, Staddon GE, Atkins RM. Algodystrophy and osteoporosis after tibial fractures. J Bone Joint Surg Br 1993;75(3):450–452. [PubMed: 8496220]

Sawamura S, Kingery WS, Davies MF, Agashe GS, Clark JD, Kobilka BK, Hashimoto T, Maze M. Antinociceptive action of nitrous oxide is mediated by stimulation of noradrenergic neurons in the brainstem and activation of [alpha]2B adrenoceptors. J Neurosci 2000;20(24):9242–9251. [PubMed: 11125002]

Schuligoi R, Amann R. Differential effects of treatment with nerve growth factor on thermal nociception and on calcitonin gene-related peptide content of primary afferent neurons in the rat. Neurosci Lett 1998;252(2):147–149. [PubMed: 9756343]

Sevcik MA, Ghilardi JR, Peters CM, Lindsay TH, Halvorson KG, Jonas BM, Kubota K, Kuskowski MA, Boustany L, Shelton DL, Mantyh PW. Anti-NGF therapy profoundly reduces bone cancer pain and the accompanying increase in markers of peripheral and central sensitization. Pain 2005;115(1–2):128–141. [PubMed: 15836976]

Shelton DL, Zeller J, Ho WH, Pons J, Rosenthal A. Nerve growth factor mediates hyperalgesia and cachexia in auto-immune arthritis. Pain 2005;116(1–2):8–16. [PubMed: 15927377]

Sintzoff S, Sintzoff S Jr, Stallenberg B, Matos C. Imaging in reflex sympathetic dystrophy. Hand Clin 1997;13(3):431–442. [PubMed: 9279547]

Skoff AM, Adler JE. Nerve growth factor regulates substance P in adult sensory neurons through both TrkA and p75 receptors. Exp Neurol 2006;197(2):430–436. [PubMed: 16300761]

Skoff AM, Resta C, Swamydas M, Adler JE. Nerve growth factor (NGF) and glial cell line-derived neurotrophic factor (GDNF) regulate substance P release in adult spinal sensory neurons. Neurochem Res 2003;28(6):847–854. [PubMed: 12718437]

Svensson P, Cairns BE, Wang K, Arendt-Nielsen L. Injection of nerve growth factor into human masseter muscle evokes long-lasting mechanical allodynia and hyperalgesia. Pain 2003;104(1–2):241–247. [PubMed: 12855334]

Thompson SW, Dray A, McCarson KE, Krause JE, Urban L. Nerve growth factor induces mechanical allodynia associated with novel A fibre-evoked spinal reflex activity and enhanced neurokinin-1 receptor activation in the rat. Pain 1995;62(2):219–231. [PubMed: 8545148]

Vaneker M, Wilder-Smith OH, Schrombges P, Oerlemans HM. Impairments as measured by ISS do not greatly change between one and eight years after CRPS 1 diagnosis. Eur J Pain 2006;10(7):639–644. [PubMed: 16300975]

Weber M, Birklein F, Neundorfer B, Schmelz M. Facilitated neurogenic inflammation in complex regional pain syndrome. Pain 2001;91(3):251–257. [PubMed: 11275381]

Zimmermann M. Ethical guidelines for investigations of experimental pain in conscious animals. Pain 1983;16:109–110. [PubMed: 6877845]

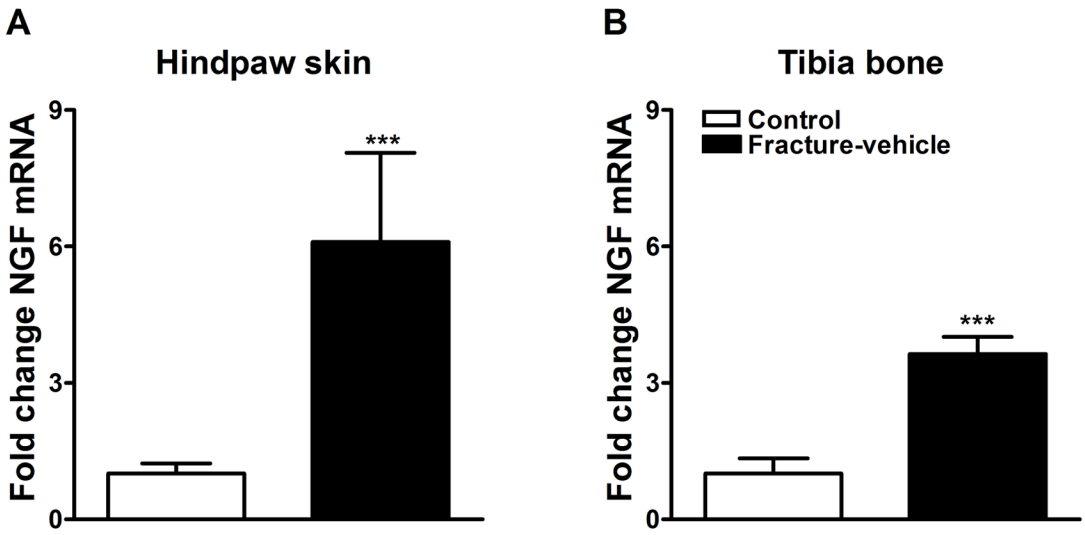

Figure 1.

NGF mRNA levels were measured by real-time PCR in hindpaw skin (panel A) and proximal tibia (panel B) in control and fracture rats. At 4 weeks after fracture NGF expression was increased in the hindpaw skin (n = 16 per cohort) and in the bone (n = 8 per cohort). $^{***}P <$ 0.001 for fracture *vs.* control values.

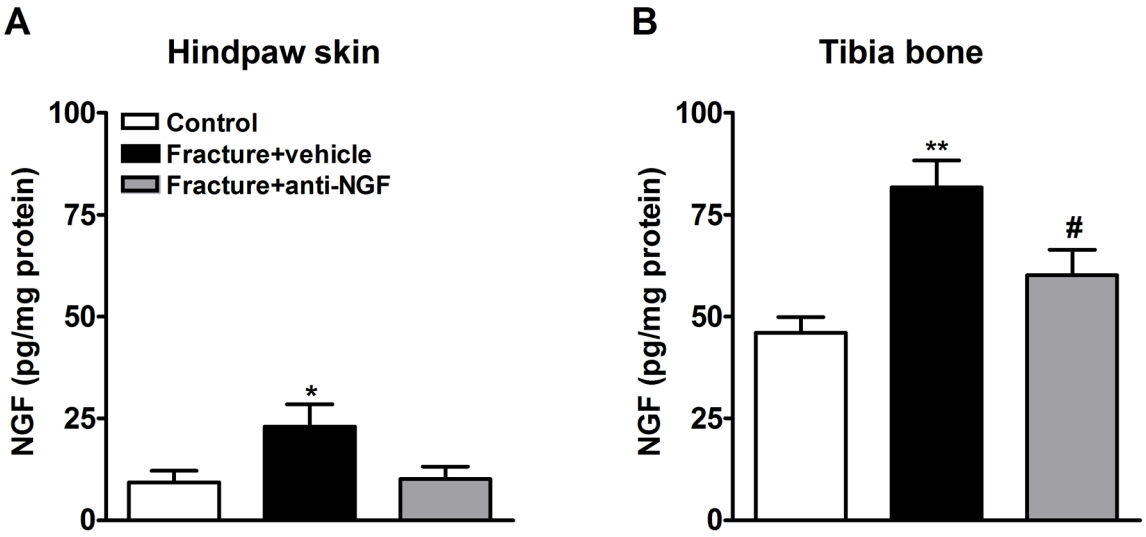

Figure 2.

After baseline testing, the right distal tibia was fractured and the hindlimb casted for 4 weeks. Anti-NGF antibodies or vehicle were injected on day 17 and day 24 after fracture. NGF protein levels were determined by enzyme immunoassay in rat hindpaw skin (A) and tibia bone (B). At 4 weeks after fracture NGF protein levels were increased in the hindpaw skin (A) and bone (B), relative to control rats (n = 8). Anti-NGF treatment blocked this elevation of NGF protein in hindlimb skin, although did not reach significance (A, n = 8) and in bone (B, n = 11). $^{*}P < 0.05$ and $^{**}P < 0.01$ fracture *vs.* control values, and $^{\#}P < 0.05$ for fracture anti-NGF treatment *vs.* fracture vehicle treatment.

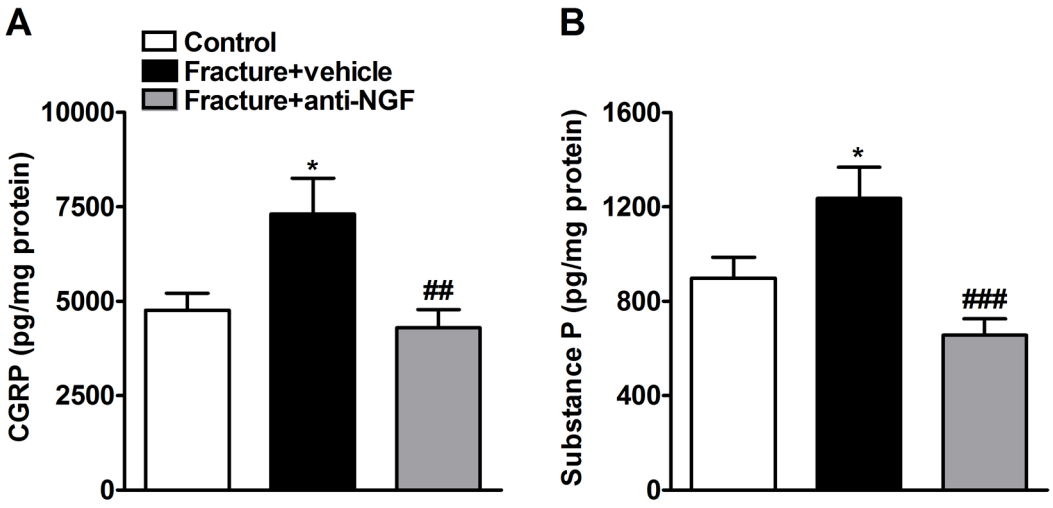

Figure 3.

CGRP (A) and SP (B) protein levels in the ipsilateral sciatic nerve were determined by enzyme immunoassay at 4 weeks after fracture. Fracture increased CGRP (n = 9) and SP (n = 9) protein levels relative to controls (n = 8), and anti-NGF antibodies blocked this fracture-induced increase in CGRP (A) (n = 12) and SP (B) (n = 12). $^{*}P < 0.05$ for fracture *vs.* control values, $^{\#\#}P < 0.01$ and $^{\#\#\#}P < 0.001$ for fracture anti-NGF treatment *vs.* fracture vehicle treatment.

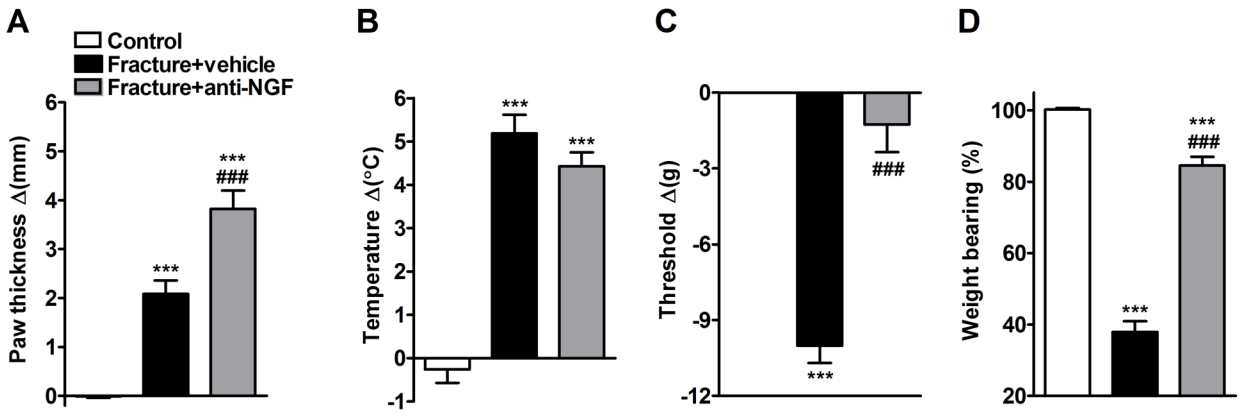

Figure 4.

Four weeks post-fracture anti-NGF treatment increased hindpaw edema (A), slightly diminished warmth (B), and reversed the hindpaw mechanical allodynia (C) and the hindlimb unweighting (D) that developed after fracture. Measurements for (A), (B), and (C) represent the difference between the fracture side and the contralateral paw, thus a positive value represents an increase in thickness or temperature on the fracture side, a negative value represents a decrease in mechanical nociceptive thresholds on the affected side. Measurements for (D) represent weight bearing on the fracture hindlimb as a ratio to 50% of bilateral hindlimb loading, thus a percentage lower than 100% represents hindpaw unweighting. $^{***}P < 0.001$ fracture *vs.* control values, and $^{###}P < 0.001$ fracture anti-NGF treatment (n = 22, Fracture +anti-NGF) *vs.* fracture vehicle treatment (n = 18, Fracture + vehicle).

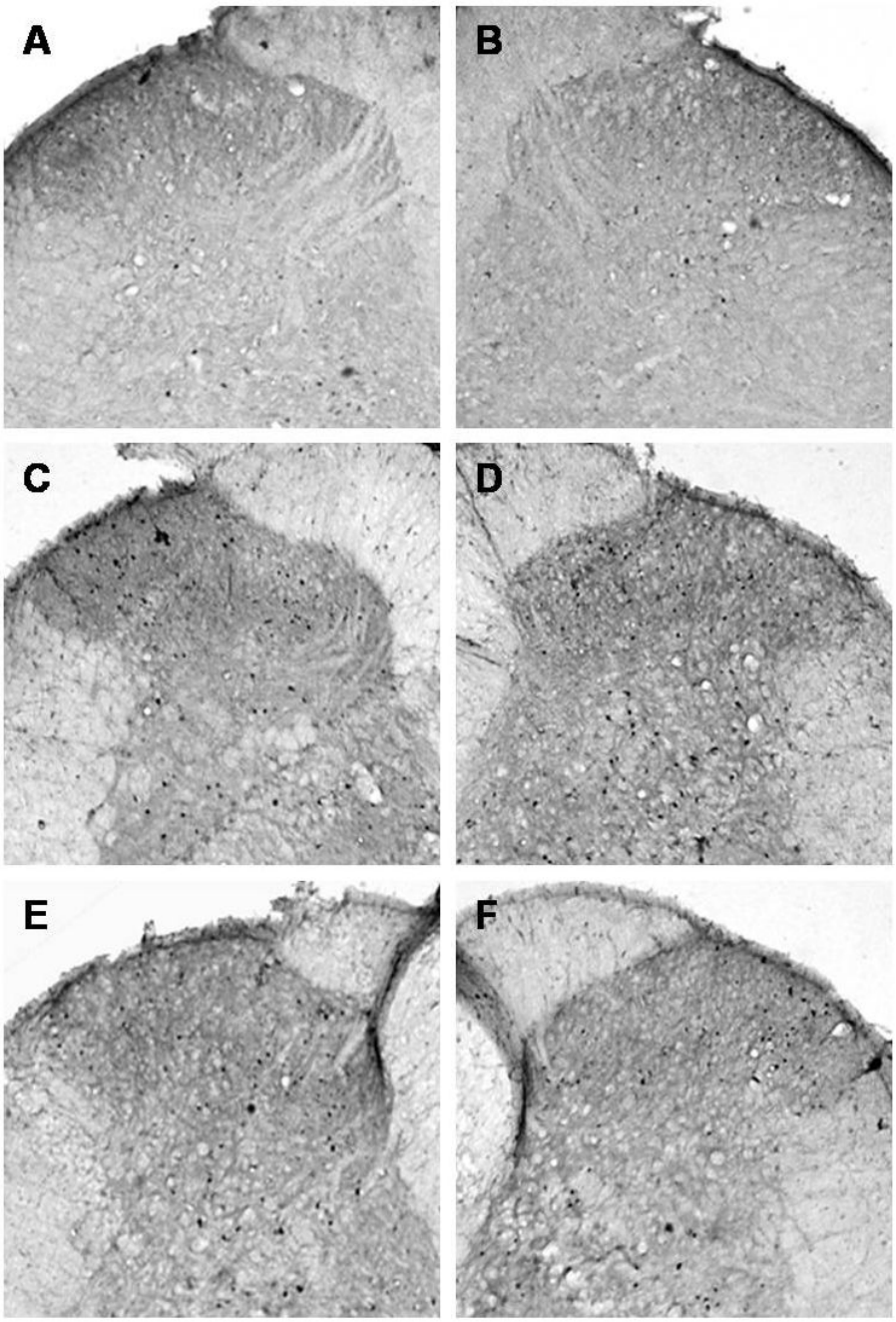

Figure 5.

Microphotographs illustrate the distribution of Fos-IR neurons in the lumbar (L4-L5 segments) spinal cord dorsal horn. All images of the spinal cord were captured with a 4X objective. Panels A and B demonstrate the right and left sides, respectively, of a control rat spinal cord section. Panels C and D demonstrate the ipsilateral and contralateral sides, respectively, of a tibia fracture rat treated with vehicle. A dense Fos immunostaining can be seen in the superficial laminae (I and II) and through the deep laminae in the ipsilateral (C) and in the contralateral dorsal horn (D). Treatment with anti-NGF antibodies partially blocked the fracture-induced increase in Fos-IR in the ipsi- and contralateral dorsal horn (E and F respectively).

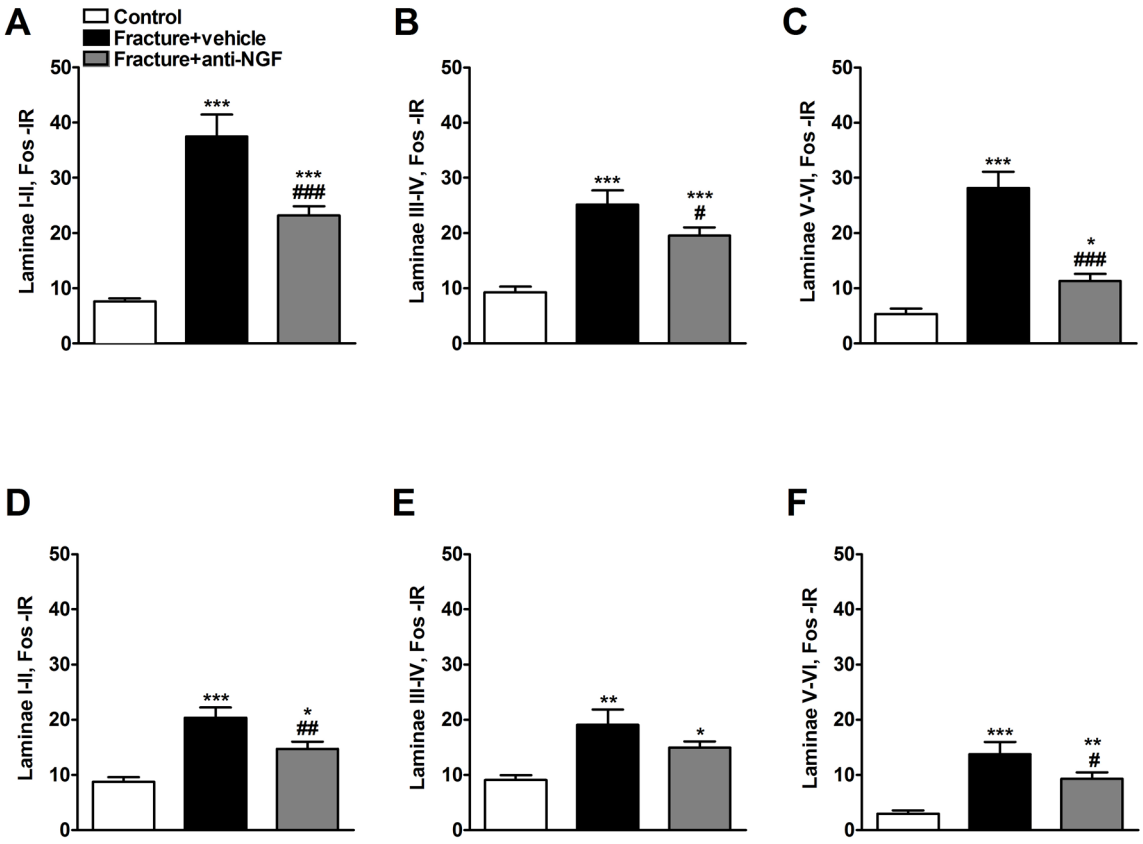

Figure 6.

Four weeks after tibia fracture and casting the L4, L5 lumbar spinal cord segments were sectioned and stained for Fos immunoreactivity. Results are expressed as the mean number of spinal Fos-IR neurons/section (± SEM), per dorsal horn laminar region (laminae I + II, III + IV and V + VI). Panels (A), (B), and (C) represent the right side of the spinal cord (ipsilateral to the fracture side), whereas panels (D), (E), and (F) represent the left side of the spinal cord (contralateral to the fracture side). There was a significant bilateral increase in Fos expression through dorsal horn laminae I-VI after fracture. Treatment with anti-NGF antibodies (n = 9, Fracture + anti-NGF) significantly decreased fracture induced spinal Fos expression, compared to the vehicle treated fracture rats (n = 6, Fracture+vehicle) through laminae I-VI ipsilaterally (A, B and C) and in laminae I-II and V-VI contralaterally (D and F). $^{*}P < 0.05$, $^{**}P < 0.01$, $^{***}P < 0.001$ fracture *vs.* control group (n = 6), and $^{\#}P < 0.05$, $^{\#\#}P < 0.01$, $^{\#\#\#}P < 0.001$ fracture anti-NGF antibodies *vs.* fracture vehicle treatment.

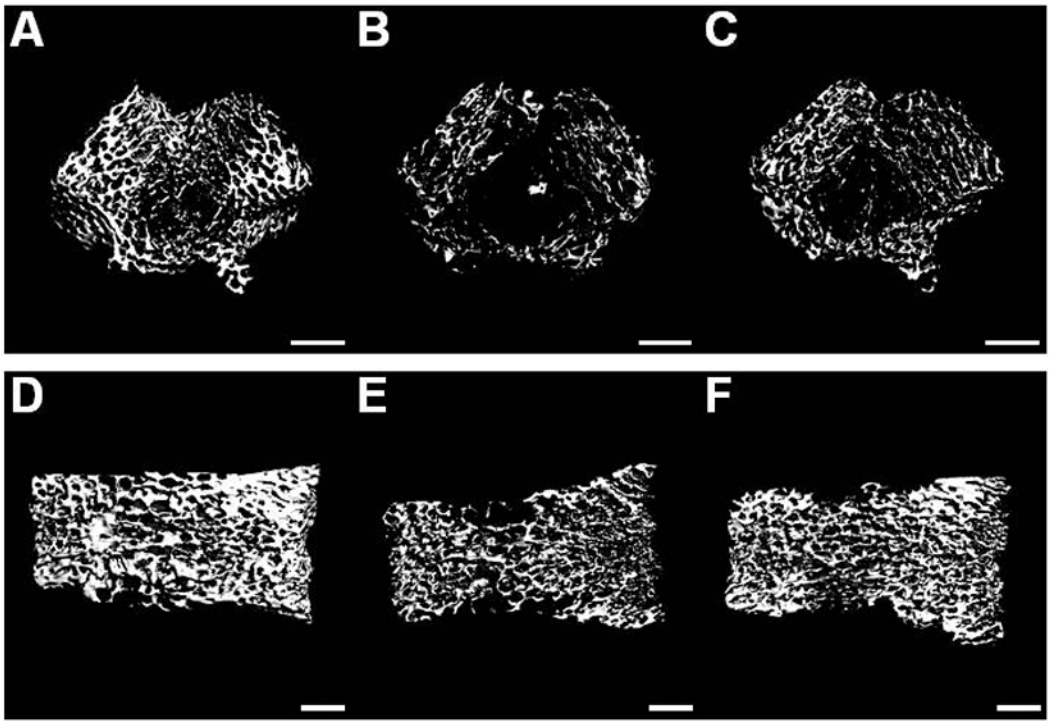

Figure 7.

After the right tibia was fractured and the hindlimb casted for 4 weeks the rats were sacrificed and the bilateral distal femurs and L_4 vertebrae were collected for *ex-vivo*μCT scanning. Three dimensional μCT images of the ipsilateral distal femur (A, B, C) and L_4 vertebra (D, E, F) illustrating changes in the trabecular bone compartment at 4 weeks after tibia fracture. Scans A and D are from a control rat; B and E are from a fracture rat treated with vehicle; and C and F are from a fracture rat treated with anti-NGF antibodies. There was a marked regional loss of trabecular bone after tibia fracture (B, E), which was partially inhibited by anti-NGF treatment (C). White bar represents 1 mm.

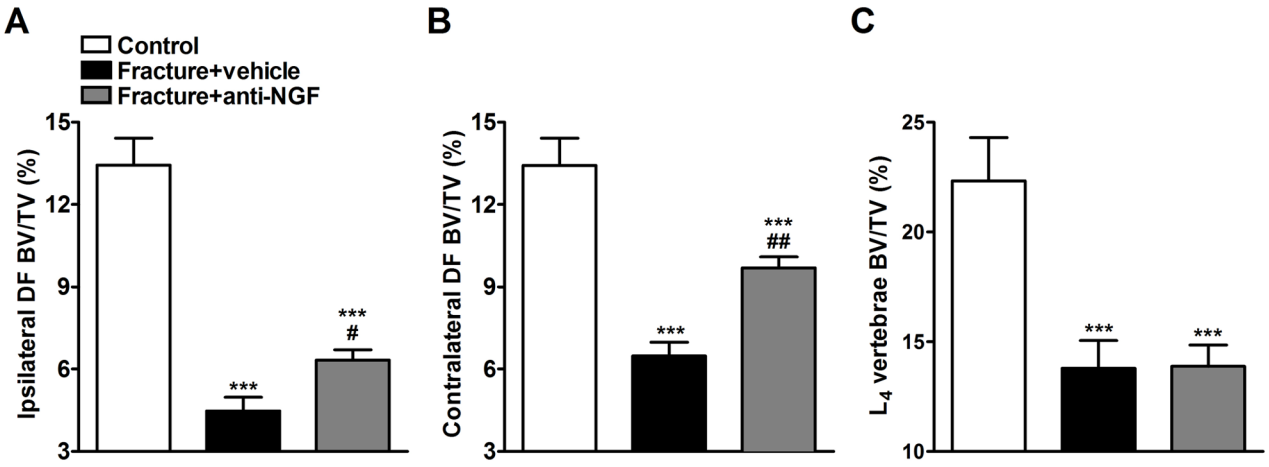

Figure 8.

There was extensive trabecular bone loss in the ipsilateral (A) and contralateral (B) distal femur, as well as in the L_4 vertebra (C) compared to control rats (n = 9 per cohort). Anti-NGF treatment partially reversed trabecular bone loss in distal femur, but not in lumbar vertebrae (Fracture +anti-NGF), relative to the vehicle treated fracture rats (Fracture + vehicle). $^{***}P < 0.001$ *vs.* control group, and $^{\#}P < 0.05$, $^{\#\#}P < 0.01$ fracture anti-NGF *vs.* fracture vehicle treatment.

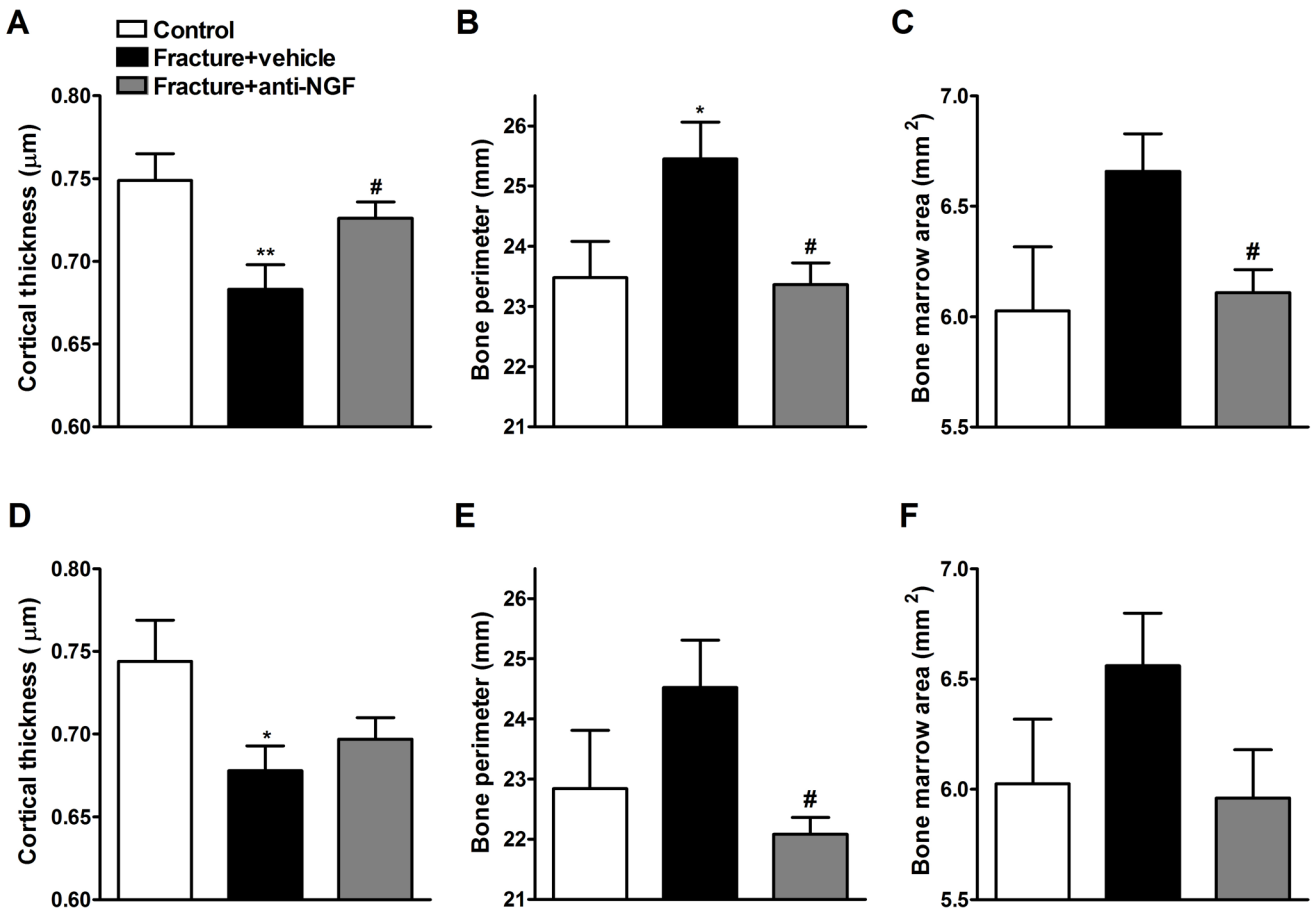

Figure 9.

Femurs were also scanned bilaterally by μCT in the middle femur region (midfemur) for cortical bone evaluation at 4 weeks post-fracture. Panels (A), (B), and (C) represent the right midfemur (ipsilateral to the fracture side), whereas panels (D), (E), and (F) represent the left midfemur (contralateral to the fracture side) regions. Fracture decreased cortical thickness (CTh, A and D), increased bone perimeter (BPm, B and E) and bone marrow area (BMAr, C and F) bilaterally (n = 18). Anti-NGF treatment (n = 22) partially restored CTh ipsilaterally (A), reversed the increase in BPm bilaterally (B and E) and the increase in BMAr ipsilaterally (C) compared to fracture vehicle group. $^{*}P < 0.05$, $^{**}P < 0.01$ fracture vehicle *vs.* control rats (n = 16), and $^{\#}P < 0.05$ fracture anti-NGF antibodies *vs.* fracture vehicle treatment groups.

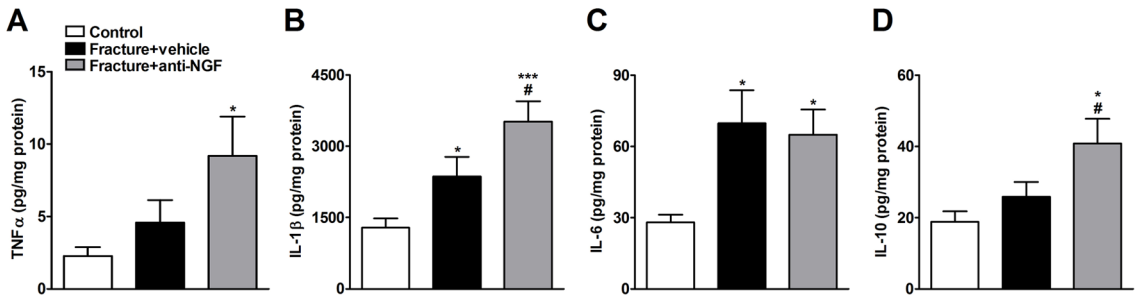

Figure 10.

Cytokine TNFα (A), IL-1β (B), IL-6 (C) and IL-10 (D) production in hindpaw skin was measured by Bio-Plex bead suspension array. Tibia fracture induced a significant increase in IL-1β (B) and IL-6 (C) cytokine levels compared to control rats. Anti-NGF treatment (Fracture + anti-NGF) induced a significant increase in all four cytokines relative to control rats and a substantial elevation was observed in IL-1β and IL-10 cytokine levels relative to the vehicle treated fracture rats (Fracture + vehicle). Data are expressed as mean values (pg/mg protein) ± S.E. (n = 8 per cohort); $^{*}P < 0.05$ and $^{***}P < 0.001$ *vs*. control rats, and $^{\#}P < 0.05$ for fracture anti-NGF *vs.* fracture vehicle groups.